Understanding Acoustoplasticity through Dislocation Dynamics Simulations

K.W. Siu and A.H.W. Ngan[§]

Department of Mechanical Engineering, The University of Hong Kong,

Pokfulam Road, Hong Kong, P.R. China

[§]Corresponding Author, email: hwngan@hku.hk

Abstract

The acoustoplastic effect in metals is routinely utilized in industrial processes involving forming, machining and joining, but the underlying mechanism is still not well understood. There have been earlier suggestions that dislocation mobility is enhanced intrinsically by the applied ultra-sound excitation, but in subsequent deliberations it is routinely assumed that the ultra-sound merely adds extra stresses to the material without altering its dislocation density or intrinsic resistance to deformation. In this study, dislocation dynamics simulation is carried out to investigate the interactions of dislocations under the combined influence of quasi-static and oscillatory stresses. Under such combined stress states, dislocation annihilation is found to be enhanced leading to larger strains at the same load history. The simulated strain evolution under different stress schemes also resembles closely certain experimental observations previously obtained. The discovery here goes far beyond the simple picture that the ultra-sound effect is merely an added-stress one, since here, the intrinsic strain-hardening potency of the material is found to be reduced by the ultra-sound, through its effect on enhancing dislocation annihilation.

Keywords: Acoustoplasticity; ultrasonic softening; dislocation dynamics simulation; dislocation annihilation

1. Introduction

Acoustoplasticity, also known as the Blaha effect [1] or ultrasonic softening, is manifested as a reduction in the quasi-static stress required to deform a material (i.e. softening) as ultrasonic vibration is simultaneously applied. Acoustoplasticity is utilized in many industrial processes to deform, cut or join metals [2-9], and is a phenomenon widely investigated over the last sixty years using tensile, compression or other test modes [1, 10-28]. In general, acoustoplasticity exhibits the following characteristics:

(i) The softening is found to become more prominent as the ultrasonic intensity increases [12-19].

(ii) The effect is an instantaneous one, meaning that the softening happens immediately upon the application of ultrasonic vibration, and diminishes once the vibration is switched off [12-14].

(iii) However, not withstanding (ii) above, residual softening or hardening compared to the state before ultrasound excitation may happen after the ultrasound has been switched off. Residual softening is more often observed [29-33], whereas residual hardening can sometimes be observed if the ultrasonic intensity is high [13, 34, 35].

(iv) The ultrasound frequency over a wide range does not have significant effects on the softening [13, 18, 19].

In terms of the mechanism behind acoustoplasticity, Langenecker [13] proposed that the ultrasound leads to enhancement of mobility of dislocations by

increasing their ability to overcome obstacles. There has also been the suggestion that, in terms of producing softening, certain equivalence would exist between the ultrasound intensity and temperature [13]. This equivalence arises from the experimental observation that, in metals which softens upon heating, the application of ultrasound of a suitable intensity will produce the same softening as that due to heating up the specimen to a given temperature [13]. However, the actual measured temperature rise in the specimen due to the application of the ultrasound is usually insignificant [13-15, 17, 23, 27, 28], implying that the ultrasound induced softening is not due simply to the general heating by the ultrasound. That the equivalence between ultrasound intesnity and temperature may not be a general phenomenon can also be seen in materials which harden on heating, such as Ni_3Al, which exhibits the well-known flow stress anomaly [36]. If the ultrasound-temperature equivalence exists in such a material, then application of ultrasound while the material is being deformed would produce hardening instead of softening. Fig. 1 shows the Vickers hardness as well as the corresponding indent diagonal lengths measured from a series of indentation tests on an Al sample as well as a Ni_3Al sample, both of which were subjected to ultrasound vibration of different amplitudes during the indentation at room temperature (experimental procedures were similar to those reported in [37]. It can be seen that in both materials, significant softening happened on increasing ultrasound amplitude. The strength of Al is well known to decrease on increasing temperature, and so it may be argued that the ultrasound softening observed here is similar to thermal softening [13]. However, for Ni_3Al, room temperature, which was the test temperature, is well within the strength anomaly regime, i.e. it's strength increases on increasing temperature [36], and so the results here indicate that no apparent equivalence between ultrasound excitation and temperature eixsts in Ni_3Al,

because in this material ultrasound excitation leads to softening but temperature rise leads to strengthening.

As further steps beyond Langenecker's original suggestion that ultrasound increases the mobility of dislocations [13], detailed models to predict ultrasound softening have been proposed, by exploiting the $\dot{\varepsilon}-\tau$ relation between strain rate ($\dot{\varepsilon}$) and stress (τ) [38-40]. In this group of investigations, the material's $\dot{\varepsilon}-\tau$ relation is assumed to be unchanged by the ultrasound, and so with the presence of an ultrasound stress field, smaller static stresses are required to deform the material at the same strain rate, compared to the case without simultaneous application of ultrasound. Using a power-law form $\dot{\varepsilon} \propto \tau^m$, Tanibayashi [38] showed that the reduction $\Delta\tau$ in the static applied stress τ_a due to the application of an oscillatory stress $\tau_v \sin \omega t$ (t = time) to achieve the same strain rate without the oscillatory stress is given as:

$$(\tau_a - \tau_i)^m = \left\langle (\tau_a - \tau_i - \Delta\tau + \tau_v \sin \omega t)^m \right\rangle \tag{1}$$

where $\langle \cdots \rangle$ means the time average of the quantity $(\cdots)$ and τ_i is an internal friction stress. In arriving at Eqn. (1), parameters such as the stress exponent m, the prefactor in the stress dependence of the strain rate as well as the friction τ_i, were assumed not to change by the ultrasound. In particular, since the prefactor depends on dislocation structure as characterized by, for example, the dislocation density, the latter was also assumed not to change by the ultrasound. Along a similar line, Malygin [39, 40] employed the Arrhenius-rate-law form $\dot{\varepsilon} \propto \exp[-(H_0 - V\tau)/kT]$ as a $\dot{\varepsilon}-\tau$ relation to predict the ultrasound softening, where V is the activation volume, H_0 the stress-free activation energy, and k and T have their usual meanings. Again, the pre-exponential factor, which reflects the dislocation structure, is assumed not to change by the ultrasound. On a similar basis, there has also been a group of work employing the

finite-element method to compute the ultrasound softening effect, by assuming the same yield surface applies with and without ultrasound excitation [23, 24, 26]. Another group of work models acoustic softening effects by considering the modification of the yield surface and/or reduction in strain hardening [41-44]. A reduction in the interfacial friction has also been proposed as a cause of ultrasonic softening [23, 24] but this idea was subsequently rejected based on finite-element predictions [28] as well as the experimental findings that ultrasonic softening was still observed even when friction was negligible [25, 26].

The works summarized above were all continuum descriptions of ultrasound softening, and surprisingly, dislocation-level microstructural investigations on ultrasonically excited metals have been very rare. Westmacott and Langenecker [45] discovered that subgrains formed in ultrasonically excited aluminium, and in a recent study [37], we further confirmed that in aluminium, very extensive subgrain formation followed simultaneous application of ultrasonic vibration and quasi-statically applied load. Preliminary dislocation dynamics (DD) simulations also showed that dislocation annihilation is greatly enhanced by a combination of oscillatory and quasi-static stress [37]. These results are inconsistent with the assumption of an invariant $\dot{\varepsilon}-\tau$ relation in the models by Tanibayashi [38] and Malygin [39, 40], or the assumption of an unchanged yield surface as in the finite-element models [23, 24, 26], since if subgrain formation takes place or the dislocation density changes, both the $\dot{\varepsilon}-\tau$ relation as well as the yield surface should also change. Daud et al. [28] actually found that the experimentally observed softening in aluminum was greater than the finite-element predicted value assuming an unchanged yield surface, implying that the assumption of invariant yield surface is not correct. A satisfactory understanding of ultrasound softening should therefore embrace the

ultrasound's effect on dislocation density reduction or subgrain formation as experimentally observed [37, 45], but so far, no such model exists. In this paper, we aim to develop such a model, by simulating using DD the effects of the ultrasound stress wave amplitude on the evolution of strain and strain rate under different quasi-statically applied stress schemes.

2. Simulation model and schemes

2.1 DD model and operating principle

The present DD simulations were two-dimensional (2D). Three-dimensional calculations are more realistic for small quantities of dislocations, but the computational efforts increase tremendously to an intractable extent as the total line length of dislocations in the simulation cell grows. Here, our purpose is to simulate large quantities of dislocations, so as to gain a statistically averaged understanding of the interactive behaviour between dislocations at different ultrasound stress levels. For this reason, the present DD simulations were 2D, and the simulation region was a square with side length of 2000 Burgers vectors, where the Burgers vector is the basic length unit here. In the simulation scheme used, initially 2000 parallel screw dislocations are randomly generated in the simulation region as in [37]. In 2D DD, the convenient choice is either a pure screw dislocation setting or a pure edge one, and pure screw is used here because dislocation production, which is an important feature in the reality of 3D, can be more easily incorporated as discussed in section 2.3 below. In 2D, two independent slip systems are needed for general plasticity, and so in the present simulations, there are two glide planes perpendicular to each other. That the two slip planes are perpendicular is just a convenient choice, and in the future, other geometries can be investigated. The applied shear stress acts on a plane at 45^{o} to both

slip planes so as to produce equal resolved stress on them. Dislocations gliding on one can cross slip onto the other according to a protocol to be described later in sections 2.2 and 2.3. The initial dislocations have their signs (i.e. right-hand or left-hand screw) and original glide planes randomly assigned. The force, velocity and displacement of each dislocation are calculated for every time step, and these quantities are renewed in next time step according to dislocation's new positions.

2.2 Detailed simulation scheme

Two types of forces contribute to the Peach-Koehler forces acting on the dislocations: (i) external forces due to the quasi-static and/or oscillatory shear stresses applied at 45^o to the sides of the simulation region as illustrated in [37], and (ii) the pair-wise elastic interaction forces between dislocations, the magnitude of which is given as $\mu b_i b_j /(2\pi r_{ij})$, where μ is the shear modulus, b_i and b_j are the Burgers vectors of an interacting pair, and r_{ij} is their distance. The total force on each dislocation is calculated as the summation of (i) and (ii), and the glide force and cross-slip force are calculated as components of the total force on the glide plane and cross-slip plane respectively. The dislocations are assumed to glide with velocity v according to $v \propto f^m$, where f is the glide force. Molecular dynamics simulations have illustrated that inertia effects of dislocations are important in the GHz load frequency range [46], but the usual frequency range used in ultrasonics is many orders of magnitude lower at ~10^4 Hz, and this should not be high enough to make inertia effects important. To give an order-of-magnitude estimation, Bitzek and Gumbsch [46] concluded that the rest mass M of a dislocation is a fraction of atomic mass per length of the Burgers vector which translates to ~1×10^{-16} kg/m for a typical metal, and the drag coefficient c is on the order of 1×10^{-5} Pa-s. The ratio of inertia force to drag

force is therefore $(M\omega/c) \sim 10^{-16} \times 2\pi \times 10^{4}/10^{-5} \sim 10^{-6}$, which is minute ($\omega$ here is angular frequency). For this reason, inertia effects are ignored in the present simulations. Periodic boundary conditions are also used so that if a dislocation slips out of the simulation box on one side, it re-enters from the opposite side.

Sinusoidal oscillatory stresses of different amplitudes were applied on top of quasi-static stresses to simulate the ultrasound excitation effects. In the results presented below, unless stated otherwise, the period of the oscillatory stress was 20 time steps, but in one set of simulations, the period was varied to see its effect on the deformation. Each simulation typically ran for 9000 time steps (the unit of the time step is explained below). The strain rate $\dot{\varepsilon}$ and strain change $\Delta\varepsilon$ at each simulation step of duration Δt were calculated as

$$\dot{\varepsilon} = \rho b \bar{v} , \tag{2}$$

$$\Delta\varepsilon = \rho b \bar{v} \times \Delta t \tag{3}$$

where ρ is the dislocation density in the simulation region, b the magnitude of Burgers vector and $\bar{v}$ the average velocity of dislocations in the deformation direction. The accumulated strain at each time step was calculated by integrated $\Delta\varepsilon$ up to that time step.

Normalized parameters were used in the simulations and their relations to real parameters are explained here. In the following, $(\tilde{\bullet})$ denotes the normalized value of the parameter $(\bullet)$. First, stresses τ are normalized by $\mu/2\pi$ where μ is the shear modulus, i.e.

$$\tilde{\tau} = \tau/(\mu/2\pi) . \tag{4}$$

As mentioned before, the real dislocation velocity is assumed to obey a power law

$$v = v_o \left(\tau / \tau_o\right)^m \tag{5}$$

where v_o / τ_o^m is a lumped constant and *m* is set at 10. In the simulation programme, the normalized velocity law used is $\tilde{v} = \tilde{\tau}^m$, and so with eqn. (4), the normalized velocity is related to the real velocity by

$$\tilde{v} = \frac{v}{v_o}\left(\frac{2\pi\tau_o}{\mu}\right)^m . \tag{6}$$

Distances *x* are normalized by the Burgers vector, i.e.

$$\tilde{x} = x / b , \tag{7}$$

and hence from eqn. (6), the simulation time step $\Delta\tilde{t}$ is related to the real time step Δt by

$$\Delta\tilde{t} = \frac{v_o}{b}\left(\frac{\mu}{2\pi\tau_o}\right)^m \Delta t . \tag{8}$$

Since strains are dimensionless, the simulated strains are the same as the real strains, but since strain rates have dimensions of 1/time, by eqn. (8), the simulated strain rates are related to the real ones by

$$\tilde{\dot{\varepsilon}} = \frac{b}{v_o}\left(\frac{2\pi\tau_o}{\mu}\right)^m \dot{\varepsilon} . \tag{9}$$

2.3 Cross slip, annihilation and generation

Dislocations are allowed to cross slip onto the other slip plane with a certain random probability (fixed at, say, between 0 and 15%) when the ratio of the cross-slip force to the glide force exceeds 5. The actual condition for cross-slip is material dependent and is difficult to specify generically, and so in this exercise, the random probability was varied between 0 and 15% to see the corresponding effects, and the critical stress ratio was set at 5 as a nominal value. Annihilation of dislocations occurs

whenever two oppositely signed dislocations are at a distance shorter than one Burgers vector.

For dislocation generation, Frank-Read sources are 3-D structures and they cannot be represented appropriately in 2-D simulations. However, in the real, 3-D situation, dislocations can also multiply when they cross slip [47-49]. For this reason, in the present 2-D simulations, a new dislocation dipole is allowed to be generated at a random probability of 1% whenever the cross-slip criterion is met for an existing dislocation. The new dipole lays on the cross-slip plane of the triggering dislocation, which is then kept on the original glide plane without cross-slip. This structure resembles the multiplication mechanism in 3-D by cross slip [48-50], in which the cross-slipped segment of the parent dislocation develops into a daughter dislocation loop, while the linking segments on either side remain on the original glide plane. In the current 2-D representation, the dipole represents the generated dislocation loop, and the original dislocation represents the linking segments.

2.4 Stress equivalence consideration

One goal of the present work is to compare with Tanibayashi's [38] stress-equivalence condition in Eqn. (1). Tanibayashi's original equations in his work [38] dealt with cases in which the oscillatory stress amplitude is not large enough to cause reversal of the total superimposed stress in the half cycle when the oscillatory stress opposes the static stress, and if such reversal is allowed in the time integration, Eqn. (1) becomes

$$\frac{1}{\pi}\int_{-\pi/2}^{\pi/2} sign(1-p+q\sin\theta)\times\left|1-p+q\sin\theta\right|^{m} d\theta = 1 \qquad (10)$$

where $p=\Delta\tau/\tau_a$, and $q=\tau_v/\tau_a$. The solved p-q relation is shown in Fig. 2. As an example, according to this stress-superposition principle, the quasi-static stress should

be reduced by 0.32 unit if 0.5 unit of oscillatory stress is superimposed, in order to keep the same strain rate as that achieved by 1 unit of static stress alone. It is this model that the present DD simulations were designed to compare with. To gain statistically averaged understanding, in this part of the work, 100 simulations were run for each set of parameters with different randomly generated initial configurations. The period of the oscillatory stress was fixed at 20 time steps.

3. Results

Fig. 3(a) shows the simulated stress-strain curves of three different stress schemes in which the quasi-statically applied stress is ramped up linearly from 0 to 2 units over the 9000 simulation time steps, and the cross-slip probability and probability of new dislocation generation are kept at 0.1 and 0.01 respectively. Here, the curve with square symbols represents the situation with the quasi-static stress only, the curve with triangular symbols represents the situation with an oscillatory stress of amplitude of 0.5 unit applied on top of the quasi-static stress throughout the simulation, and the curve with circular symbols represents the situation in which the oscillatory stress (also of amplitude of 0.5 unit) is superimposed on the quasi-static stress only between 2000 and 5000 steps. It can be seen that with the simultaneous application of the oscillatory stress (curve with triangular symbols), the strain at any given stress is larger than the situation with the quasi-static stress only (curve with square symbols). The simultaneous application of the oscillatory stress clearly produces softening here. Also, as can be seen from the inset in Fig. 3(a) which shows the enlarged view in a small strain region from strain of 0 to 0.005, in the situation described by the curve with circular symbols, softening happens immediately when

the oscillatory stress is switched on at step 2000 at which the quasi-static stress is 0.4 unit. Further time steps beyond 2000 see the approach of the curve with circular symbols towards the curve with triangular symbols, meaning that the softening behaviour after switching on of the oscillatory stress quickly catches up with that in the situation when the oscillatory stress is applied continuously from the onset. Returning to the main panel in Fig. 3(a), when the oscillatory stress is switched off at step 5000 at which the quasi-static stress is 1.1 units, the stress-strain curve with circular symbols departs from the curve with triangular symbols and reverts back towards the curve with square symbols, meaning that the softening due to the oscillatory stress is lost once the latter is switched off. The results here resemble the experimental observation that softening happens upon the application of ultrasonic vibration, and stops when the vibration is switched off [12-14]. It can be seen that the number of dislocations remaining is significantly less when oscillatory stress is applied, and the dislocation density remains high if no oscillatory stress is applied at all. Fig. 3(b) shows the number of dislocations remaining versus the time step under the three stress conditions. The dislocation population with the simultaneous application of the oscillatory stress (curve with triangular symbols) is significantly smaller than the situation with the quasi-static stress only (curve with square symbols). This is due to the fact that the oscillatory stress promotes dislocation annihilation [37]. In the half cycle when the oscillatory stress reinforces the quasi-static stress, the total stress is large and hence the dislocations can travel long distances over unit time. This allows them to explore new environments and this increases the chance of annihilation [37]. In the case of the intermittent application of the oscillatory stress (curve with circular symbols), enhanced annihilation takes place immediately after the oscillatory stress is switched on at step 2000. When the oscillatory stress is switched

off at step 5000, the speed of annihilation reduces immediately, resulting in a sharp cusp in the curve with circular symbols at step 5000. In Fig. 3(a), it can be seen that the curve with circular symbols catches up with the curve with square symbols at strain of about 0.5 and exceeds the latter beyond this strain, and so this case corresponds to a small extent of residual hardening [13, 34, 35]. Fig. 3(c) and (d) show the results of using the same set of stress schemes but the probability of new dislocation generation is increased to 0.1 and 0.18 respectively. As the probability of new dislocation generation increases the curve with circular symbols can no longer surpass the curve with square symbols after the vibration has been switched off. This corresponds to residual softening [29-33], and is due to the greater ease of dislocation generation. Fig. 3(e) and (f) show the number of dislocations remaining versus the time step corresponding to Fig. 3(c) and (d) respectively. Although in these cases the increased dislocation generation probability causes a momentary surge in dislocation content, at large simulation steps the overall effect is still annihilation of dislocations, and the overall number of dislocations remaining after 9000 steps is smaller than in the case of Fig. 3(b). The application of oscillatory stress either throughout or intermittently during the deformation produces a slight increase in dislocation content compared to the case when no oscillatory stress is applied at all, and this explains the residual softening as seen in Fig. 3(c) and (d).

Fig. 4 shows the simulated results as the applied static stress is kept constant at 1 unit throughout the simulation, and the cross-slip probability and probability of new dislocation generation are kept at 0.1 and 0.01 respectively. This resembles a condition of creep when the applied stress is kept constant, albeit the simultaneous application of an oscillatory stress. In addition to creep, the simulated situation here also resembles indentation with a feedback loop to increase the load to keep the mean

stress underneath the indenter (i.e. the hardness) constant. As reported previously [37] (and also shown in Fig. 1), ultrasound softening of aluminium was observed in indentation experiments, although a feedback loop was not used in the experiments. In Fig. 4(a), again, three stress schemes are compared: (i) static stress only (curve with square symbols), (ii) static stress plus oscillatory stress of amplitude 0.5 unit throughout (curve with triangular symbols), and (iii) the situation in which the oscillatory stress (also of amplitude of 0.5 unit) is superimposed on the static stress only between 2000 and 5000 steps (curve with circular symbols). It can be seen from the strain versus time curve in Fig. 4(a) that addition of the oscillatory stress leads to faster creep, and also, the effect is instantaneous upon switching on of the oscillatory stress in the case of the curve with circular symbols. Upon switching off of the oscillatory stress at the 5000^{th} step, the strain also slows down immediately, and the strain rate (the slope of the curve) drops to a value close to the situation when no oscillatory stress is applied at all (the curve with square symbols). The strain itself does not revert back to the situation with no oscillatory stress because the strain change during the switching on of the oscillatory stress is an irreversible effect. Fig. 4(b) shows the number of dislocations remaining versus the time step under the three stress conditions. The oscillatory stress enhances dislocation annihilation and the curve with circular symbols drops rapidly from the 2000^{th} to the 5000^{th} step during which the oscillatory stress is switched on. Upon switching off of the oscillatory stress at and beyond the 5000^{th} step, the rate of decrease of the dislocation density becomes similar to the curve with square symbols. From Fig. 4(a) it can be seen that the strain rate in the case of the curve with circular symbols after switching off of the oscillatory stress at the 5000^{th} step is slightly less than that of the curve with square symbols at the same time step, indicating a residual hardening effect due to the previously

applied oscillatory stress, which lowers the dislocation content as seen from Fig. 4(b). Fig. 4(c) shows the effect of the probability of new dislocation generation on the residual hardening or softening. Here, different dislocation generation probabilities were used in parallel runs of the simulation similar to that shown in Fig. 4(a), and the average slope m_1 and m_2 of the curves with square and circular symbols respectively immediately after the 5000^{th} step were noted. The ratio m_2 / m_1 is taken as an indication of residual hardening if it is smaller than 1, and of residual softening if it is larger than 1. As can be seen from Fig. 4(c), when the probability of new dislocation generation is smaller than 0.38, residual hardening happens, and when the probability of generation exceeds 0.38, residual softening occurs. Fig. 4(d) shows the change in the number of dislocations versus time when the probability of dislocation generation is at a very high value of 0.5. It can be seen that if the oscillatory stress is applied throughout the simulation, there will be a net accumulation of dislocations, whereas in the other two schemes there will be an overall exhaustion of dislocations. The dislocation number after the 5000^{th} step in the curve with circular symbols is slightly larger than that in the curve with square symbols, and this accounts for the residual softening in Fig. 4(c) at this condition.

Fig. 5 shows more simulated creep situations with a static stress applied, in addition to an oscillatory stress. Here, for each oscillatory stress amplitude simulated, the magnitude of the static stress satisfies the stress equivalence principle in eqn. (10), so that if the equivalence principle is correct, then the strain rate produced with the simultaneous application of the oscillatory stress will be the same as that produced by 1 unit of static stress alone. Also, for each stress condition, 100 replicas with randomly generated initial dislocation configurations were simulated, and Fig. 5(a)

and (b) show the number of dislocations remaining after 9000 steps versus the simulated oscillatory stress amplitude (lower scale) or the static stress (upper scale), with and without dislocation generation respectively. The error bars here account for one standard deviation in the ensemble of 100 simulations at each condition. In all stress states simulated in Fig. 5(a,b), dislocation annihilation is allowed and even if dislocation generation is also allowed as in Fig. 5(a), the number of remaining dislocations is lower than the initial 2000, indicating the effects of dislocation annihilation during the deformation. In Fig. 5(a) when dislocation generation is allowed, the remaining dislocation population first increases with the oscillatory stress amplitude until the latter reaches 0.7 unit, and then it drops for higher values of oscillatory stress amplitude. The rise in the remaining dislocation population before the 0.7 unit of oscillatory stress also increases as the cross-slip probability increases, and noting that in the present simulation protocol dislocation generation can only follow cross slip, this rise is readily explained as a consequence of the enhanced dislocation generation as the cross-slip probability increases. Also, when the cross-slip probability is set to zero, no dislocation generation is allowed to happen, and so the remaining dislocation population can only drop. Fig. 5(b) shows that without new dislocation production more dislocations are annihilated with higher cross-slip probability. When the cross-slip probability is zero, the remaining dislocation quantity is close to a constant value in a small oscillatory stress amplitude regime, but decreases significantly when the oscillatory stress amplitude is greater than 0.4 unit. Fig. 5(c) shows the resultant strain after 9000 simulation steps versus the simulated stress state, in situations with and without dislocation annihilation and generation for comparison. In the situation when dislocation generation and annihilation are disallowed, the resultant strain increases slightly with increasing oscillatory stress

amplitude before 0.7 unit, after this amplitude the resultant strain drops significantly. This behaviour is different from that predicted from Tanibayashi's equivalence principle, which is represented as a red horizontal line in Fig. 5(c). With the dislocation content purposely barred from changing in this set of simulations, Tanibayashi's equivalence principle predicts the resultant strain to remain constant when the oscillatory stress amplitude and the static stress vary according to eqn. (10), but the current DD simulations show that this is not the case. In essence, Tanibayashi's consideration ignores the complicated group interactions between dislocations, even though their quantity is not allowed to change. When dislocation generation and annihilation are allowed to occur, the simulated resultant strain remains about constant for oscillatory stress amplitudes smaller than 0.7 unit, and decreases rapidly when the oscillatory stress increases further. The rapid decrease of strain at high oscillatory stresses is due to the corresponding reduction in the static stress so as to fulfil eqn. (10), and under such small mean stress values the dislocations simply oscillate about their equilibrium positions without producing much strain.

Fig. 6 shows the effect of the frequency of the oscillatory stress on the number of dislocations remaining after 9000 steps of simulation, with and without new dislocation generation. Data points with dislocation generation are represented by filled circles and those without dislocation generation are represented by squares. Here, the period of the oscillatory stress was varied from 20 to 200 time steps, while the oscillatory stress amplitude was maintained at 0.3 unit, and the cross-slip probability and probability of new dislocation generation were kept constant at 0.15 and 0.01 respectively. The static stress was at 0.85 unit and this also obeys eqn. (10). It is obvious that increasing the period by ten times does not have any significant

effect on the number of remaining dislocations. This agrees with the experimental observation that the ultrasound frequency over a wide range does not have significant effects on the softening [13, 18, 19].

4. Discussion

The present work is the first attempt to understand ultrasound softening using a dislocation dynamics simulation approach. Of special importance here is the discovery that the simultaneous application of an oscillatory stress on top of a quasi-static stress can significantly change the dislocation density in the material, compared to the situation with the quasi-static stress only. Unless probability of dislocation generation is very high, the more usual effect of the oscillatory stress is to reduce the dislocation density, and although experiments have revealed such an effect [37, 45], this has never been stipulated or accounted for in previous theoretical considerations of acoustoplasticity. As discussed in Section 1, previous theories of acoustoplasticity only focussed on the increased mobility of dislocations under the combined influence of the ultrasound and quasi-static stresses – an effect which may be described as an "added stress" effect. In one group of models [38-40], the dislocation density is explicitly assumed not to change by the ultrasound, and previous finite-element simulations [23, 24, 26] also assumed the yield surface to be unchanged by the ultrasound, which would not be the case if the dislocation density is affected by ultrasound.

By analysing the present simulated dislocation structures in detail, the reduction in the dislocation density with the simultaneous application of an oscillatory

stress is found to be an indirect "added stress" effect which is explained below. In the half cycle when the oscillatory stress reinforces the quasi-static stress, the total stress becomes large, and because the velocity law is of the power-law form $v \propto \tau^m$, the velocity increases tremendously. Dislocations can therefore travel very long distances to explore different environments, and this increases their chance of encountering opposite signed dislocations for annihilation to occur. In the half cycle when the oscillatory stress opposes the quasi-static stress, the dislocations are slowed down, and interestingly, this is also found to be a favourable factor for annihilation, because the periodic pause of the dislocation movements increases their chances to cross slip so that they would not easily miss further chances for annihilation with nearby dislocations on intersecting slip planes. When the probability of dislocation generation is kept low, dislocation generation cannot keep up with the enhanced annihilation and so the overall effect is a net reduction in the dislocation density, which causes the interactions amongst dislocations (i.e. strain hardening) to reduce, and this in turn leads to further increase in the dislocations' velocities. Also, in the above-discussed phenomena, the frequency of the oscillatory stress should not play a role – the frequency of reversal of the oscillatory stress should not affect the long distances covered by the dislocations in the reinforcing half cycle, nor their encounter with opposite signed dislocations for annihilation. This explains the null effect of the oscillatory stress frequency observed in Fig. 6, which also agrees with experiments [13, 18, 19].

Figs. 3 and 4 also show a residual effect induced by the oscillatory stress, and this is found to be influenced by the probability of new dislocation generation. As shown in Fig. 4(c), when this probability is low residual hardening is more likely to occur whereas higher dislocation generation probability leads to residual softening.

The residual hardening or softening effect is due to a permanent change in dislocation content during the application of the vibration. When generation rate is low, a lot of dislocations are annihilated during the oscillatory stress period, and when the oscillatory stress is switched off, the static stress alone now drives a small population of dislocations so that the strain rate is low – this corresponds to residual hardening. On the other hand, if the dislocation generation probability is made very high, the oscillatory stress can actually increase the dislocation content as shown in Figs. 3(e), 4(f) and 4(d), compared to the case without oscillatory stress. In this case, a larger population of dislocations is driven by the combined static and oscillatory stress so the strain rate is higher – this corresponds to residual softening.

The above discussion involves two opposing effects of reducing the dislocation density on strain rate. When the dislocation density is high, reducing the dislocation density produces softening because this weakens interactions amongst dislocations or strain hardening according to the Taylor effect. This is the softening effect of the oscillatory stress when the dislocation generation probability is kept low, and is also the common expectation that recovered metals with reduced dislocation densities are softer, not stronger, than work-hardened counterparts with higher dislocation densities [49]. However, when the dislocation density is already made to a low value, due, for example, to a previous cycle of oscillatory stress, a lower dislocation density situation will correspond to a smaller strain rate, or residual hardening, as compared to a higher dislocation density situation, because the dislocations are simply the “carriers” of deformation according to Eqn. (2). Reducing the dislocation density can therefore produce either a reduced strain-hardening effect when the density is high, or a reduced deformation carrier effect when density is low,

and these two opposing effects must be appreciated in order to understand the softening effect of ultrasound, versus its residual softening/hardening effect.

The simulations in this study clearly indicate the importance of dislocation annihilation as an ultrasound softening effect, in addition to the "added-stress" effect on dislocation velocity as proposed by previous researchers [38-40]. From eqn. (2), the fractional change of the strain rate is the sum of the fractional changes of the dislocation density and velocity, i.e.

$$\frac{\delta\dot{\varepsilon}}{\dot{\varepsilon}} = \frac{\delta\rho}{\rho} + \frac{\delta\overline{\upsilon}}{\overline{\upsilon}} \ , \tag{11}$$

and so at a given stress condition and microstructural state, the ratio $R = \frac{\delta\rho / \rho}{\delta\overline{\upsilon} / \upsilon}$, where the changes are due to slight perturbation of the imposed conditions, indicates the relative importance of the two factors of dislocation density and velocity. To study which factor becomes dominating, a series of simulations were run with the static stress and oscillatory stress amplitudes fixed at values ranging from 0 to 1.2 units at an increment of 0.05 unit. At each stress state, the oscillatory stress amplitude was perturbed by 0.05 unit to produce changes in the dislocation density and velocity, whereas the cross-slip probability and the probability of new dislocation generation were fixed at 0.1 and 0.01 respectively. The *R* value defined above was calculated as the average between the simulated states at the 2000^{th}, 4000^{th}, 6000^{th}, 8000^{th} and 9000^{th} step, and Fig. 7 shows the results. It can be seen that when both the static stress and the oscillatory stress are small, the ratio *R* is close to zero, meaning the change in average velocity has a dominating effect on the change in strain rate. When the stress is higher, however, the ratio is generally larger than one, meaning that the strain rate is dominated by a change in the dislocation density, due to the enhanced annihilation.

Fig. 7 clearly shows the demarcation of the effects of dislocation density and velocity on ultrasound softening, and indicates that in the high-stress regime, consideration of dislocation annihilation is much more pertinent than dislocation velocity.

Finally, a note on the relevance of the present simulations to the real time scales commonly encountered in ultrasonics is necessary. In the present work, we choose not to adopt particular values of the various material constants, but to carry out the computation with normalized physical units (see eqns. (4), (7) and (8)). This choice is due a few factors. First, some of the material constants (e.g. drag coefficient) are not known precisely, and can vary significantly between materials and dislocation mechanisms, but we just aim at a simplified model which can predict generic behaviour independent of materials. Secondly, since the simulations are 2D, relaxation and impedance of dislocations in a third dimension are not allowed, and so the stress level may not be comparable to the real 3-D case. Thirdly and most importantly, since inertia effects can be dropped as explained above, our simulations involve only one single physic, namely, that dislocations glide under stress according to $v \propto \tau^m$, and so our research question was actually to see if this simple physic can explain the key features of ultrasonic softening as summarized in points (i) to (iv) in Section I. As far as this aim is concerned, running the simulations with normalized units is sufficient, and as discussed above, the results do illustrate that the single physic of $v \propto \tau^m$ alone can explain these features of ultrasonic softening. Nevertheless, numerical evaluation of the model parameters can be done to illustrate the potential limitations. The number of time steps per stress cycle used in the present simulations is typically 20, although higher numbers were also used as shown in Fig. 6. So, in eqn. (8), if $\Delta\tilde{t} = 20$ steps correspond to $\Delta t = 5\times10^{-5}$s which is a typical

ultrasonic stress period, then the factor $(v_o/b)(\mu/2\pi\tau_o)^m$ has to be $4\times10^5\,\mathrm{s}^{-1}$. This condition can be met by letting, for example, $\tau_o = \mu/2\pi$, and $v_o \approx 10^{-4}\,\mathrm{ms}^{-1}$. If, however, the material parameters are orders of magnitude off this condition, then the simulation frequency can be out of the ultrasonic range. For example, a typical realistic condition can be $v_o \sim 10^{-5} ms^{-1}$, m ~ 10, and $\tau_o/\mu \sim 10^{-4}$ [47]. When these values are substituted into eqn. (8), 20 time steps would correspond to a real time of only $\sim 2\times10^{-36}\,\mathrm{s}$, or, the number of time steps per one ultrasonic stress cycle of $\Delta t = 5\times10^{-5}\,\mathrm{s}$ would be 10^{32}, which is not manageable in a numerical exercise. In Fig. 6, the number of time steps per stress cycle was varied from 20 to 200, and convergence of the results has already been achieved in this range. Since only one physic concerning $v \propto \tau^m$ is involved here, there is no reason that more time steps per cycle, meaning more refined computation, would produce different results.

The present work is the first of its kind, and there is ample room for future exploration with other dislocation mechanisms that may operate at different dislocation speeds. Another topic for future investigation is the relevance to metal fatigue, which also involves oscillatory stresses. Ultrasound softening is usually concerned with metal forming in which general yield takes place. On the other hand, fatigue usually involves stress levels at which general yield does not occur, and the interest as far as plasticity is concerned is at locations of stress raisers, or crack tips, where highly localized plasticity takes place with strong grain gradients. Dislocation interactions under oscillatory stresses but with strong strain gradients should be an interesting topic to investigate in the future.

5. Conclusions

A series of dislocation dynamics simulation was carried out to investigate how the density of dislocations, strain and strain rate change under different conditions of combined oscillatory and quasi-static stresses typical in acoustoplasticity. The effects of different parameters such as the oscillatory stress amplitude, frequency and ease of cross slip were investigated. The stress-strain behaviour under different stress schemes resembles typical experimental observations. Residual softening is observed with higher probability of new dislocations generation whereas lowering this value leads to residual hardening. Under combined oscillatory and quasi-static stresses, the simulations revealed that dislocation annihilation is enhanced, compared with the situation in which only the quasi-static stress acts. The resultant reduction in dislocation density weakens strain-hardening and this is an important factor to explain ultrasound softening. Tanibayashi's stress equivalence principle has been shown to be inadequate in predicting strain under different oscillatory stress, even in the situation when both dislocation annihilation and generation are suppressed. The enhanced annihilation effect was also found not to be affected by the oscillatory stress frequency over a wide range. The results here represent the first successful attempt to use dislocation-interaction based simulations to account for a number of key features of acoustoplasticity.

Acknowledgment

The work described in this paper was supported by grants from the Research Grants Council of the Hong Kong Special Administration Region, P.R. China (Project No. HKU7159/10E), as well as from the University Grants Committee (Project No. SEG-HKU06) of the Hong Kong Special Administration.

References

[1] F. Blaha and B. Langenecker, Naturwissenschaften 42 (1955) p. 556.

[2] K. C. Joshi, Weld. J. 50 (1971) p. 840.

[3] K. F. Graff, IEEE Trans. Son. and Ultrason. SU22 (1975) p. 234.

[4] A.E. Eaves, A.W. Smith, W.J. Waterhouse, D.H. Sansome, Ultrasonics 13 (1975) p. 162.

[5] H. Kreye, M. Hammerschmidt, G. Reiners, Scripta Metall. 12 (1978) p. 1059.

[6] R. Neugebauer and A. Stoll, J. Mater. Process Technol. 149 (2004) p. 633.

[7] C. Zhang, R. Rentsch, E. Brinksmeier, Int. J. Mach. Tool. Manu. 45 (2005) p. 881.

[8] B. N. Mordyuk and G. I. Prokopenko, J. Sound Vibrat. 308 (2007) p. 855.

[9] D. E. Brehl and T. A. Dow, Precis. Eng. 32 (2008) p. 153.

[10] W. Mason, Bell Syst. Tech. J. 34 (1955) p. 903.

[11] G. E. Nevill and F. Brotzen, Proc. Am. Soc. Testing Materials 57 (1957) p.751.

[12] B. Langenecker, AIAA J. 1 (1963) p. 80.

[13] B. Langenecker, IEEE Trans. Son. and Ultrason. 1 (1966) p. 1.

[14] O. Izumi, K. Oyama, Y. Suzuki, Trans. Jpn. Inst. Metals 7 (1966) p. 158.

[15] O. Izumi, K. Oyama, Y. Suzuki, Trans. Jpn. Inst. Metals 7 (1966) p. 162.

[16] G. S. Baker and S. H. Carpenter, J. Appl. Phys. 38 (1967) p. 1586.

[17] T .Endo, K. Suzuki, M. Ishikawa, Trans. Jpn. Inst. Metals 20 (1979) p. 706.

[18] H. O. K. Kirchner, W. K. Kromp, F. B. Prinz, P. Trimmel, Mater. Sci. Eng. 68 (1985) p. 197.

[19] T. Ohgaku and N. Takeuchi, Phys. Status Solidi. A 111 (1989) p. 165.

[20] K. V. Sapozhnikov and S. B. Kustov, Phil. Mag. A 76 (1997) p. 1153.

[21] K. V. Sapozhnikov, S. N. Golyandin, S. B. Kustov, Phil. Mag. A 77 (1998) p. 151.

[22] K. V. Sapozhnikov, S. N. Golyandin, S. B. Kustov, J. Van Humbeeck, R. De Batist, Acta Mater. 48 (2000) p. 1141.

[23] Z. Huang, M. Lucas, M. J. Adams, Ultrasonics 40 (2002) p. 43.

[24] Z. Huang, M. Lucas, M. J. Adams, Proc. SPIE Int. Soc. Opt. Eng. 4537 (2002) p. 445.

[25] J.-C. Hung and C. Hung, Ultrasonics 43 (2005) p. 692.

[26] J-C. Hung, Y-C. Tsai, C. Hung, Ultrasonics 46 (2007) p. 277.

[27] Y. Daud, M. Lucas, Z. Huang, Ultrasonics 44 (2006) p. e511.

[28] Y. Daud, M. Lucas, Z. Huang, J. Mater. Process Technol. 186 (2007) p. 179.

[29] J. E. Krzanowski, IEEE Trans. Compon. Hybrids Manuf. Technol. 13 (1990) p. 176.

[30] M. M. Susan, P. G. Dumitras, V. G. Iliescu, Surf. Eng. 43 (2007) p. 65.

[31] U. Geissler, M. Schneider-Ramelow, K. D. Lang, H. Reichl, J. Electron. Mater. 37 (2006) p. 173.

[32] I. Lum, H. Huang, B. H. Chang, M. Mayer, D. Du, Y. Zhou, J. Appl. Phys. 105 (2009) p. 024905.

[33] H. Huang, A. Pequegnat, B. H. Chang, M. Mayer, D. Du, Y. Zhou, J. Appl. Phys. 106 (2009) p. 113514.

[34] I. A. Gindin, G. N. Malik, I. M. Neklyudoy, O. T. Rozumnyi, Russ. Phys. J. 15 (1972) p. 192.

[35] N. A. Tyapunina, V. V. Blagoveshchenskii, G. M. Zinenkova, Y. A. Ivashkin, Russ. Phys. J. 25 (1982) p. 569.

[36] D. M. Wee and T. Suzuki, Trans. Jpn. Inst. Metals 20 (1979) p. 634.

[37] K. W. Siu and A. H. W. Ngan, Int. J. Plast. (2011). (Paper in press)

[38] M. Tanibayashi, Phys. Status Solidi A 128 (1991) p. 83.

[39] G. A. Malygin, Phys. Solid State 42 (2000) p. 69.

[40] G. A. Malygin, Phys. Solid State 42 (2000) p. 482.

[41] A. K. Rusynko, Materials Science 37 (2001) p. 671.

[42] A. Siddiq and E. Ghassemieh, Mechanics of Materials 40 (2008) p. 982.

[43] A. Siddiq and T. E. Sayed, Materials Letters 65 (2011) p. 356.

[44] A. Rusinko, Ultrasonics 51 (2011) p. 709.

[45] K. H. Westmacott and B. Langenecker, Phys. Rev. Lett. 14 (1965) p. 221.

[46] E. Bitzek and P. Gumbsch, Mat. Sci. Engg. A387-389 (2004) p. 11.

[47] D. Hull and D. J. Bacon, *Introduction to dislocations*, 4th ed., Butterworth-Heinemann, Oxford, 2001.

[48] R. E. Smallman and A. H. W. Ngan, *Physical Metallurgy and Advanced Materials*, Elsevier, 2007.

[49] U. Messerschmidt, *Dislocation dynamics during plastic deformation*, Springer, Berlin, 2010.

Figure Captions

Fig. 1. Vickers hardness and indent diagonal length versus ultrasound vibration amplitude on an Al sample (data from ref. [37]) and a Ni_3Al sample (present study) subjected to ultrasound excitation during indentation by 0.05kg load at room temperature.

Fig. 2. Relation between p and q by solving eqn. (10). p and q represent the reduction in quasi-static stress and the oscillatory stress applied to the system respectively.

Fig. 3. (a) Simulated stress-strain curves with the quasi-static stress increasing linearly from 0 to 2 units over the 9000 simulation time steps for three stress schemes: curve with square symbols – only quasi-static stress is applied; curve with triangular symbols – both oscillatory stress and quasi-static stress are applied throughout the simulation; curve with circular symbols – the oscillatory stress is applied only between the 2000^{th} and the 5000^{th} step on top of the continuous quasi-static stress acts. Cross-slip probability and probability of new dislocation generation are 0.1 and 0.01 respectively. Oscillatory stress has amplitude of 0.5 unit and period equal to 20 time steps. Inset shows the enlarged view of the regime between 0 to 0.005 strain. (b) Number of dislocations remaining versus time step under the three stress schemes. (c, d) Stress-strain curves in which the probability of new dislocation generation is changed to 0.1 (c) and 0.18 (d). (e, f) Number of dislocations remaining versus the time step corresponding to (c) and (d) respectively.

Fig. 4. (a) Strain versus time step with a static stress of 1 unit applied throughout the simulation under three stress schemes: curve with square symbols – only static stress

is applied; curve with triangular symbols – both oscillatory stress and static stress are applied throughout the simulation; curve with circular symbols – the oscillatory stress is applied only between the 2000^{th} and the 5000^{th} step on top of the continuous static stress acts. Cross-slip probability and probability of new dislocation generation are 0.1 and 0.01 respectively. Oscillatory stress has amplitude of 0.5 unit and period equal to 20 time steps. (b) Number of dislocations remaining versus time step under the three stress schemes. (c) Ratio of m_2/m_1 with different probabilities of new dislocation generation, where m_1 represents the average slope of the curve with square symbols after the 5000^{th} step and m_2 represents that of the curve with circular symbols at the same step. (d) Number of dislocations versus time step when the probability of dislocation generation is 0.5.

Fig. 5. Number of dislocations remaining in the simulation region under a continuous static stress after 9000 steps versus the amplitude of a superimposing oscillatory stress (a) with dislocation generation at a probability of 0.01, and (b) without dislocation generation. (c) Resultant strain after 9000 steps versus the simulated oscillatory stress amplitude. At each oscillatory stress amplitude, the static stress obeys eqn. (10) and is indicated at the upper horizontal axis. Period of oscillatory stress equals 20 time steps, and cross-slip probability varies as indicated by "CrossSlipProb". At each stress condition, 100 replicas with randomly generated initial configurations were simulated, and standard deviations are represented by error bars.

Fig. 6. Number of dislocations remaining after 9000 steps at a continuous static stress versus the period of a superimposing oscillatory stress with and without dislocation generation. Data points obtained with dislocation generation are represented by circles

and those without dislocation generation are represented by squares. Oscillatory stress amplitude (OsciAmp) is 0.3 unit, cross-slip probability (CrossSlipProb) is 0.15 and probability of new dislocation generation (NewDisProb) is 0.01. Static stress is 0.85 unit, which also obeys eqn. (10).

Fig. 7. Ratio $R = \frac{\delta\rho / \rho}{\delta\upsilon / \upsilon}$ plotted against different combination of static and oscillatory stresses. R is the averaged value of the 2000^{th}, 4000^{th}, 6000^{th}, 8000^{th} and 9000^{th} steps. The changes in quantities here are produced by perturbing the oscillatory stress amplitude by 0.05 unit. Data for every 0.05 unit of stress is recorded. Cross-slip probability is 0.1 and probability of new dislocation generation is 0.01.

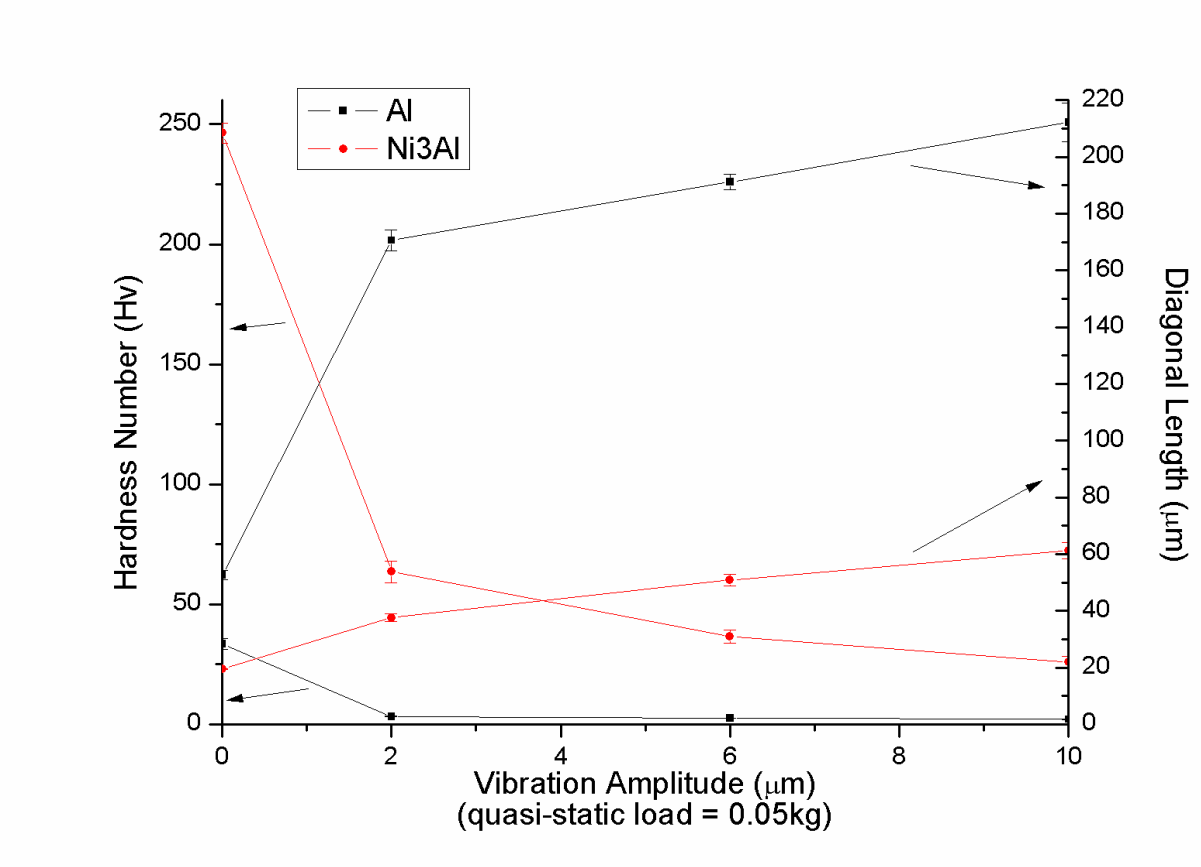
Al
Ni3Al
Hardness Number (Hv)
Diagonal Length (μm)
Vibration Amplitude (μm)
(quasi-static load = 0.05kg)
0
50
100
150
200
250
0
20
40
60
80
100
120
140
160
180
200
220
0
2
4
6
8
10

Fig. 1

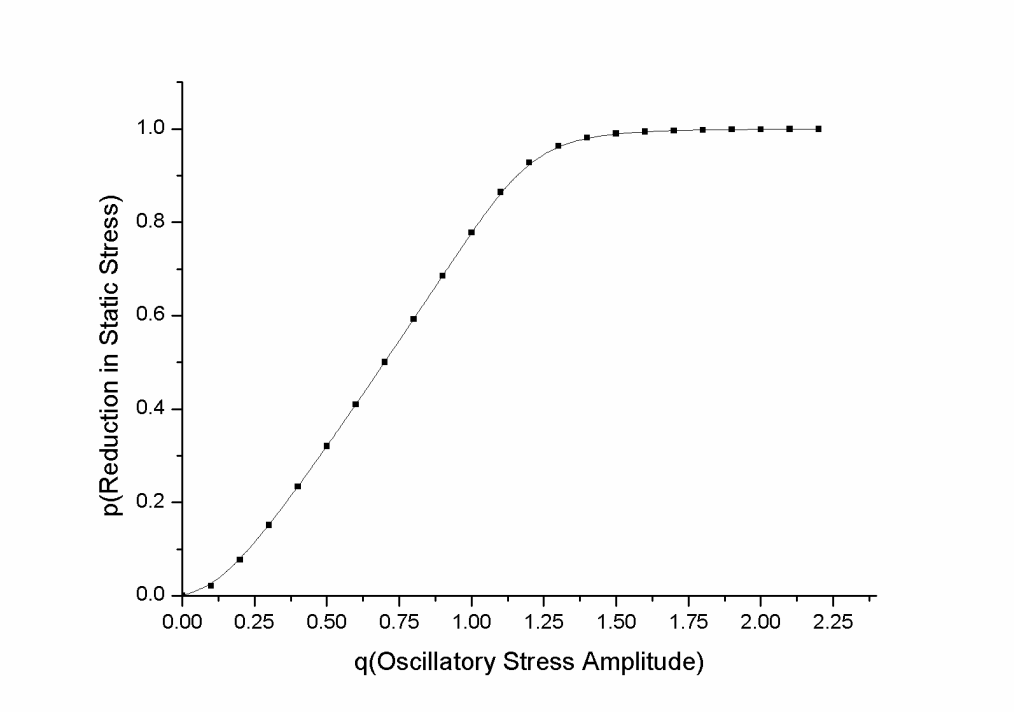
p(Reduction in Static Stress)
q(Oscillatory Stress Amplitude)
0.0
0.2
0.4
0.6
0.8
1.0
0.00
0.25
0.50
0.75
1.00
1.25
1.50
1.75
2.00
2.25

Fig. 2

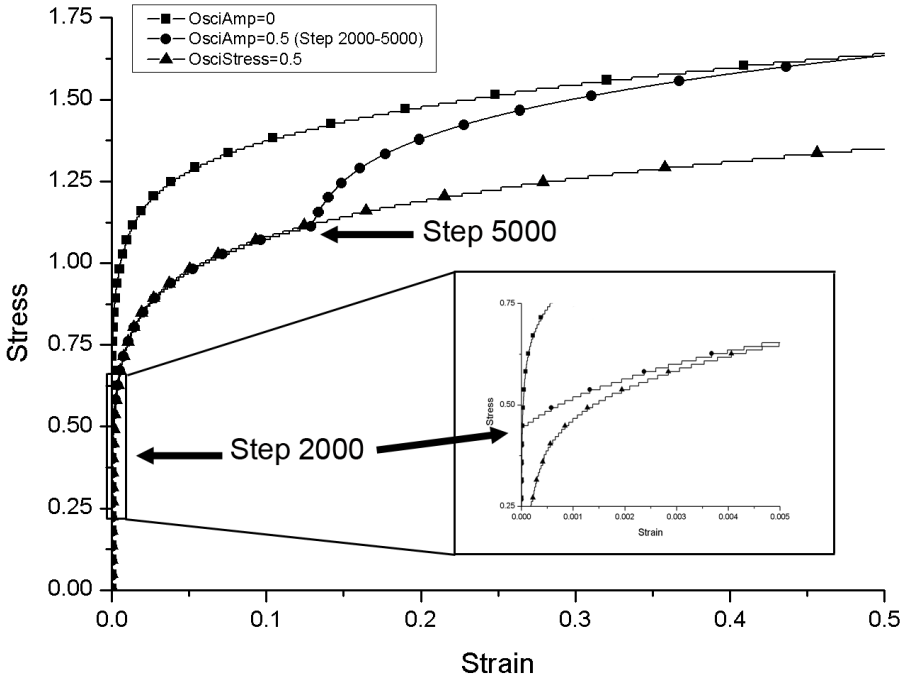
OsciAmp=0
OsciAmp=0.5 (Step 2000-5000)
OsciStress=0.5
Step 5000
Step 2000
Stress
Strain
0.00
0.25
0.50
0.75
1.00
1.25
1.50
1.75
0.0
0.1
0.2
0.3
0.4
0.5

Fig. 3(a)

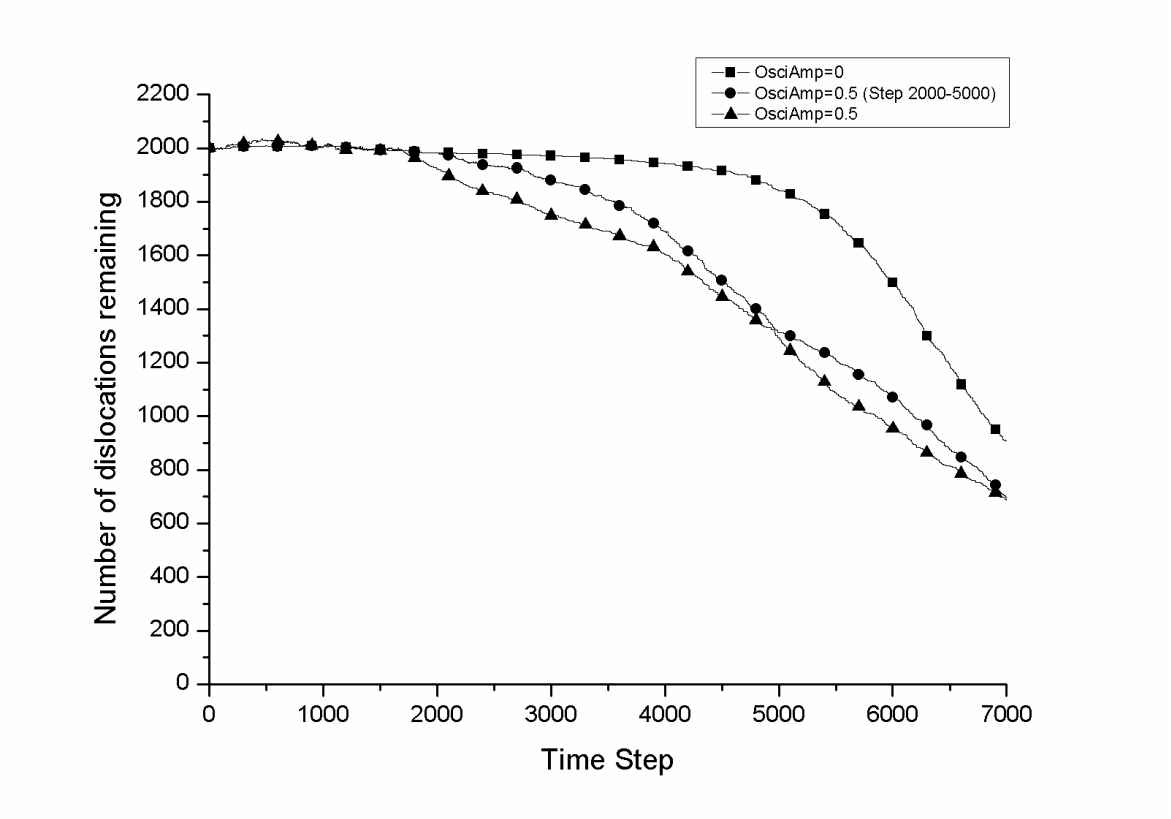
OsciAmp=0
OsciAmp=0.5 (Step 2000-5000)
OsciAmp=0.5
Number of dislocations remaining
Time Step
0
200
400
600
800
1000
1200
1400
1600
1800
2000
2200
0
1000
2000
3000
4000
5000
6000
7000

Fig. 3(b)

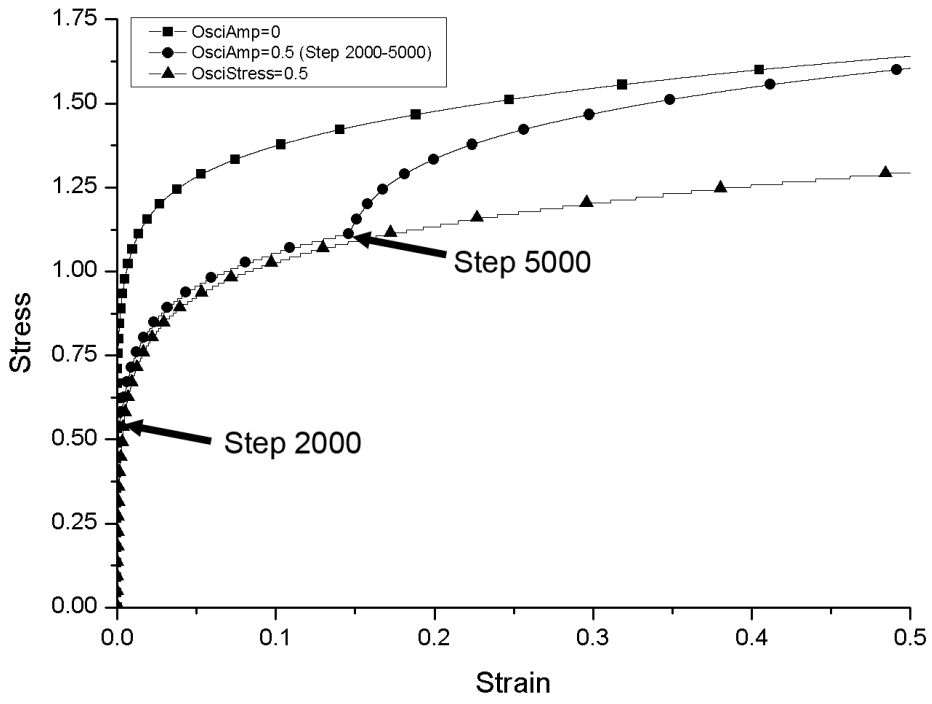
OsciAmp=0
OsciAmp=0.5 (Step 2000-5000)
OsciStress=0.5
Step 5000
Step 2000
Stress
Strain
0.00
0.25
0.50
0.75
1.00
1.25
1.50
1.75
0.0
0.1
0.2
0.3
0.4
0.5

Fig. 3(c)

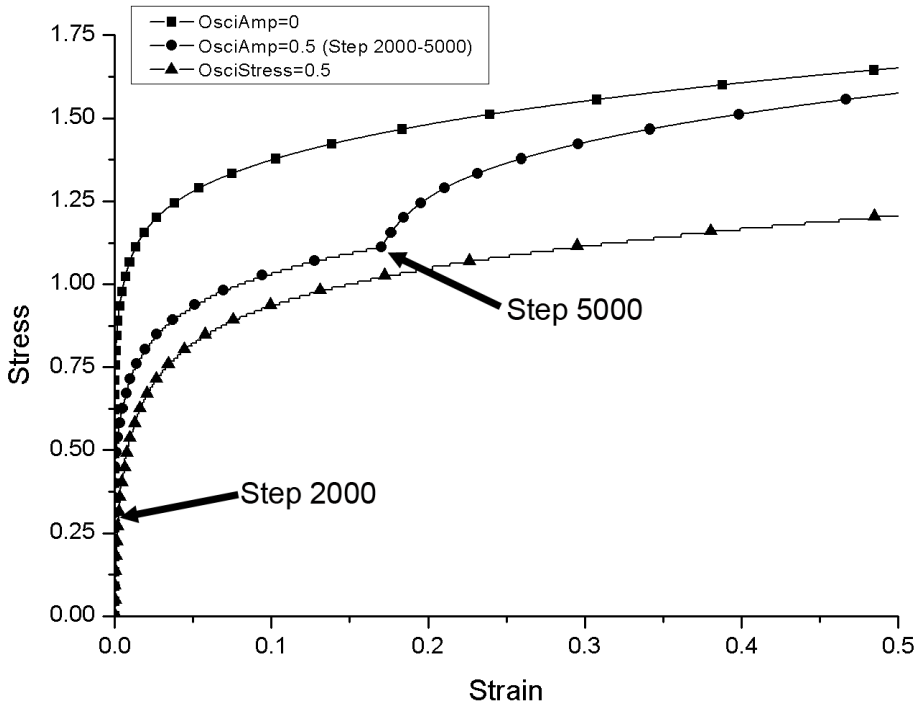
OsciAmp=0
OsciAmp=0.5 (Step 2000-5000)
OsciStress=0.5
Step 5000
Step 2000
Stress
Strain
0.00
0.25
0.50
0.75
1.00
1.25
1.50
1.75
0.0
0.1
0.2
0.3
0.4
0.5

Fig. 3(d)

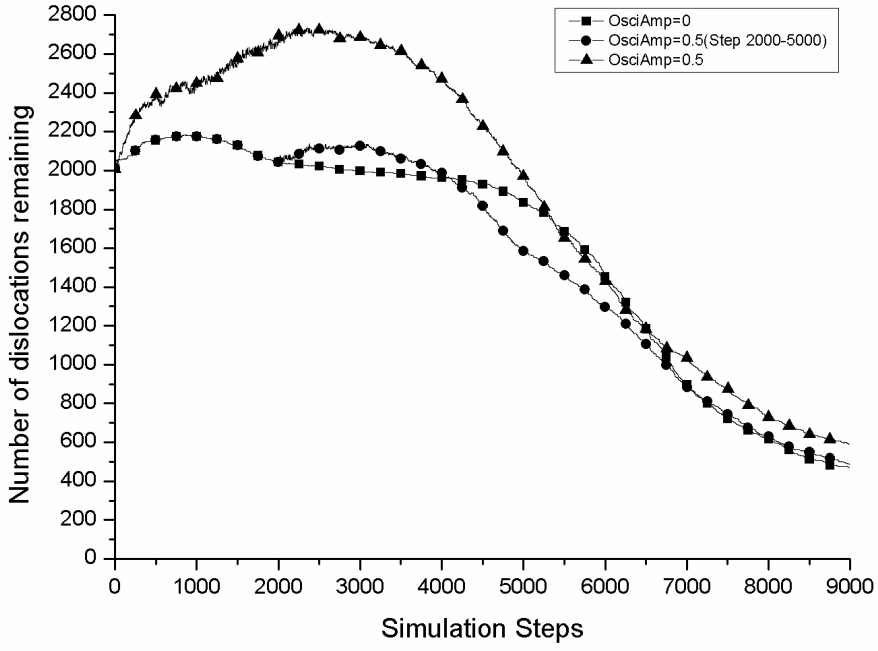
OsciAmp=0
OsciAmp=0.5(Step 2000-5000)
OsciAmp=0.5
Number of dislocations remaining
Simulation Steps
0
200
400
600
800
1000
1200
1400
1600
1800
2000
2200
2400
2600
2800
0
1000
2000
3000
4000
5000
6000
7000
8000
9000

Fig. 3(e)

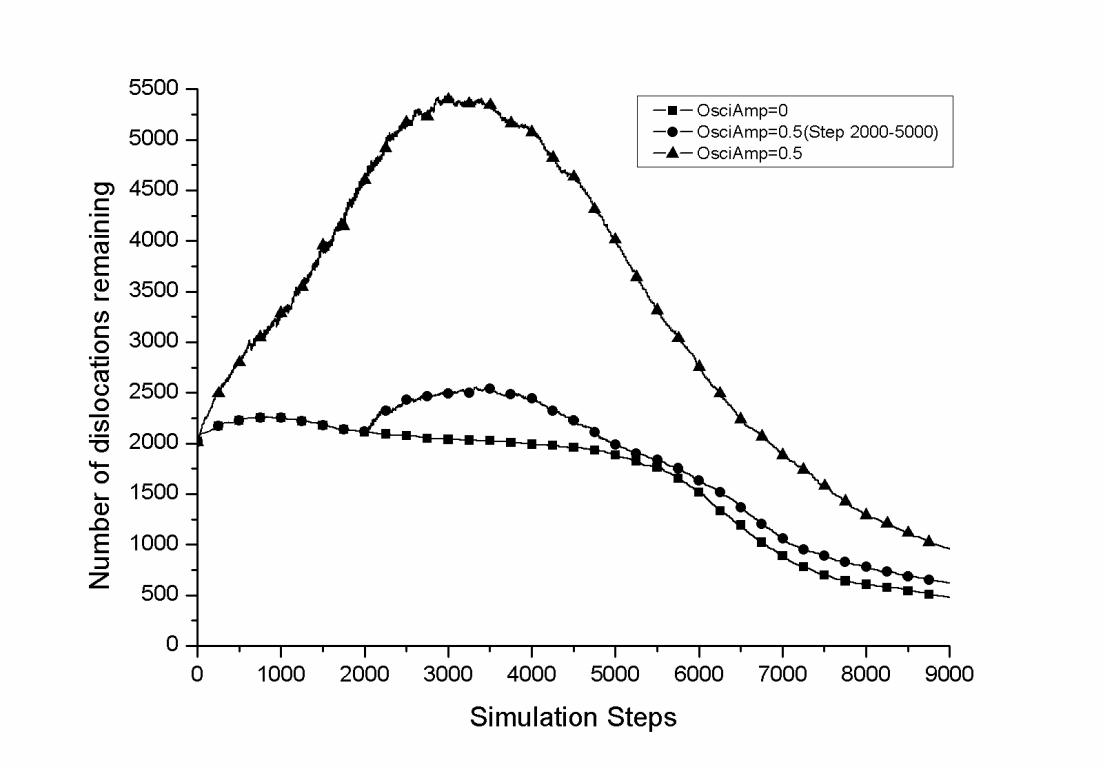
OsciAmp=0
OsciAmp=0.5(Step 2000-5000)
OsciAmp=0.5
Number of dislocations remaining
Simulation Steps
0
500
1000
1500
2000
2500
3000
3500
4000
4500
5000
5500
0
1000
2000
3000
4000
5000
6000
7000
8000
9000

Fig. 3(f)

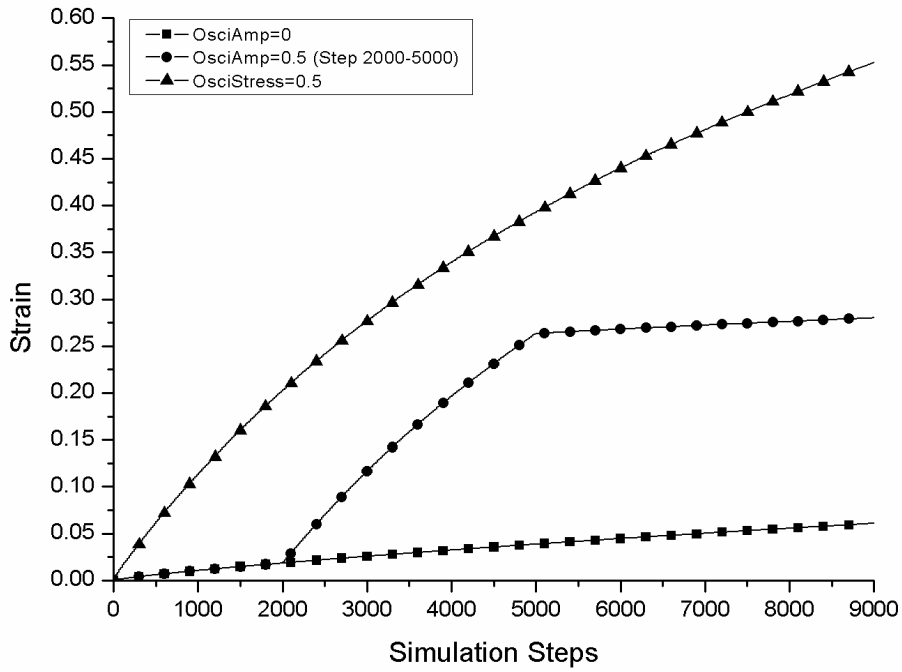
OsciAmp=0
OsciAmp=0.5 (Step 2000-5000)
OsciStress=0.5
Strain
Simulation Steps
0.00
0.05
0.10
0.15
0.20
0.25
0.30
0.35
0.40
0.45
0.50
0.55
0.60
0
1000
2000
3000
4000
5000
6000
7000
8000
9000

Fig. 4(a)

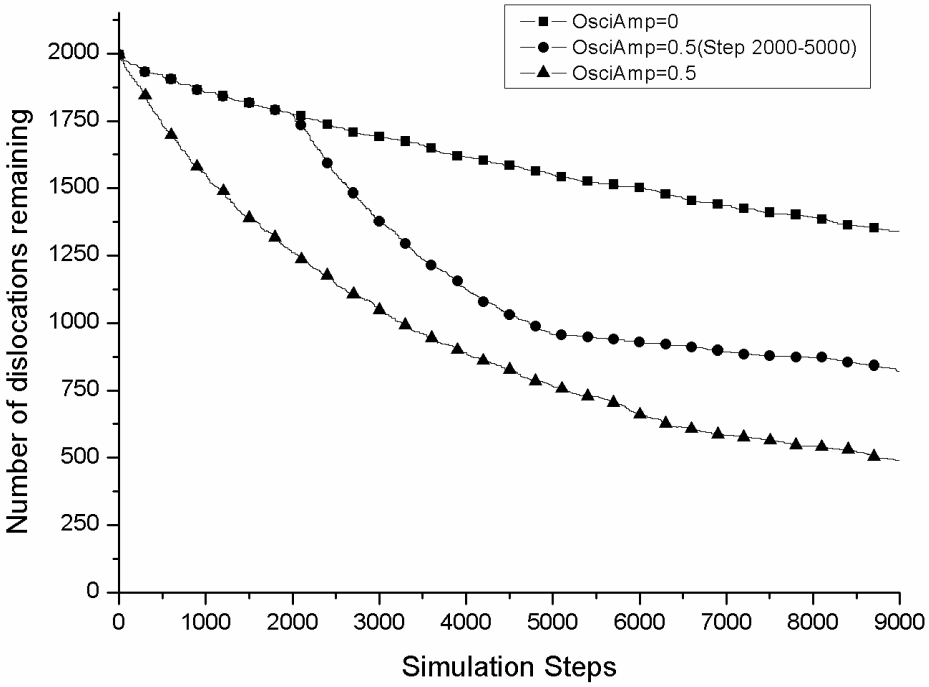
OsciAmp=0
OsciAmp=0.5(Step 2000-5000)
OsciAmp=0.5
Number of dislocations remaining
Simulation Steps
0
250
500
750
1000
1250
1500
1750
2000
0
1000
2000
3000
4000
5000
6000
7000
8000
9000

Fig. 4(b)

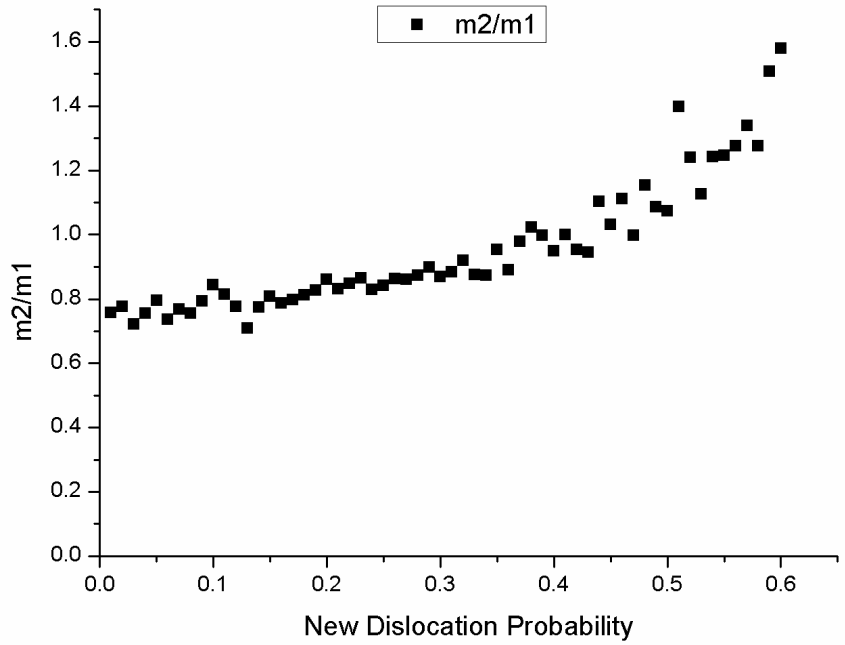
m2/m1
1.6
1.4
1.2
1.0
0.8
0.6
0.4
0.2
0.0
m2/m1
0.0
0.1
0.2
0.3
0.4
0.5
0.6
New Dislocation Probability

Fig. 4(c)

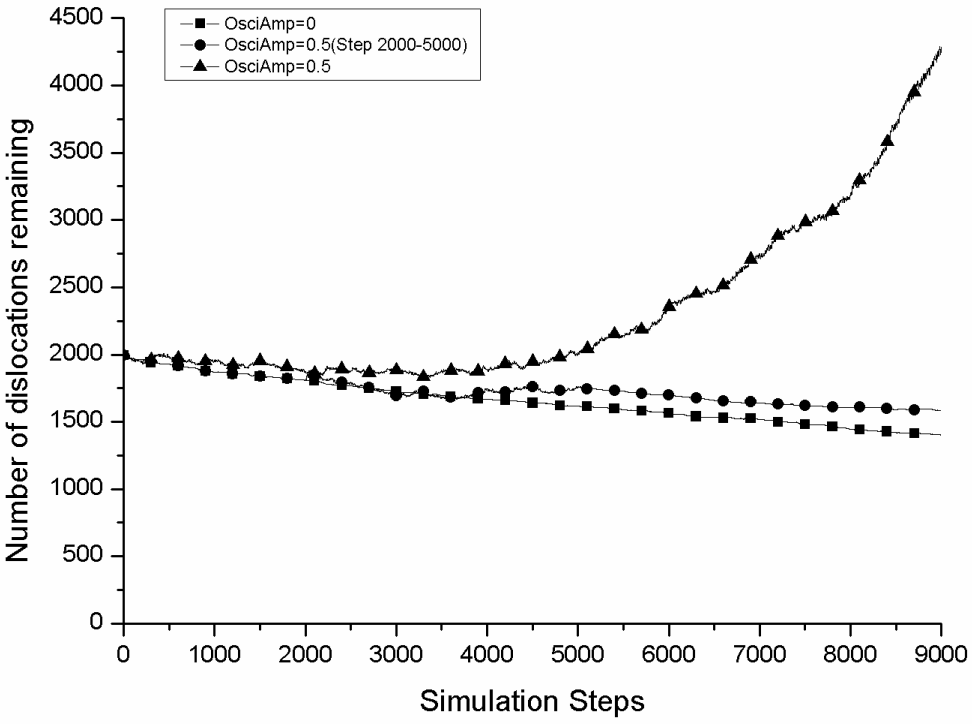
OsciAmp=0
OsciAmp=0.5(Step 2000-5000)
OsciAmp=0.5
4500
4000
3500
3000
2500
2000
1500
1000
500
0
Number of dislocations remaining
0
1000
2000
3000
4000
5000
6000
7000
8000
9000
Simulation Steps

Fig. 4(d)

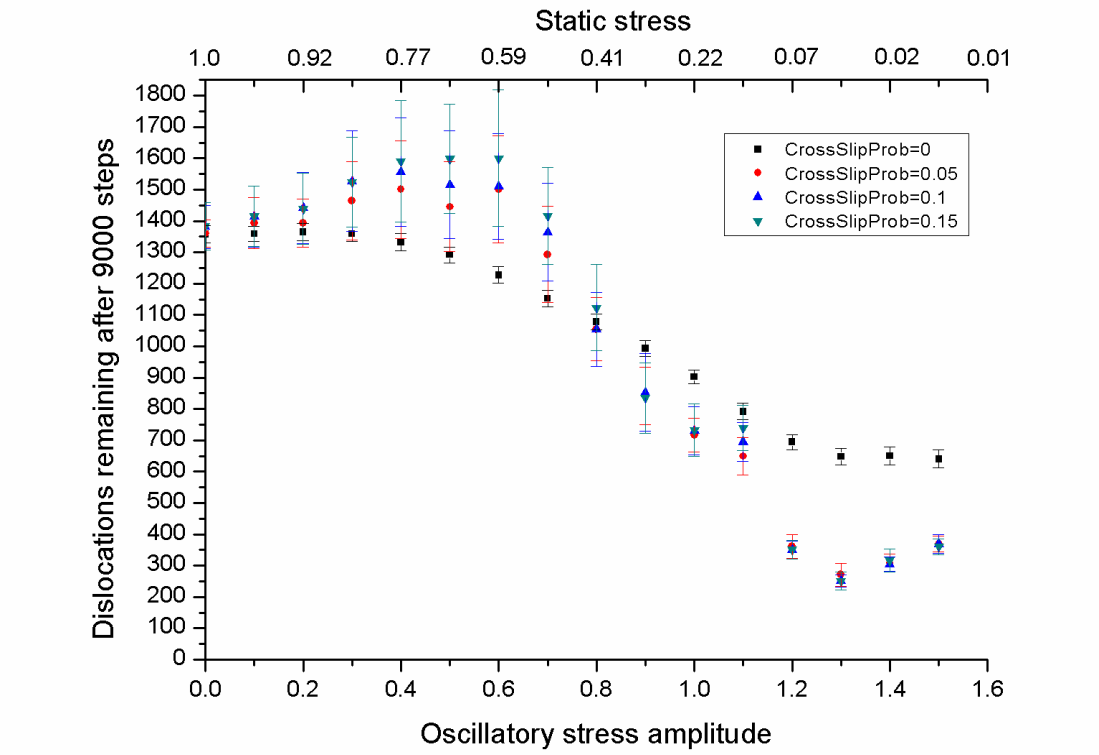
Static stress
1.0
0.92
0.77
0.59
0.41
0.22
0.07
0.02
0.01
Dislocations remaining after 9000 steps
1800
1700
1600
1500
1400
1300
1200
1100
1000
900
800
700
600
500
400
300
200
100
0
0.0
0.2
0.4
0.6
0.8
1.0
1.2
1.4
1.6
Oscillatory stress amplitude
CrossSlipProb=0
CrossSlipProb=0.05
CrossSlipProb=0.1
CrossSlipProb=0.15

Fig. 5(a)

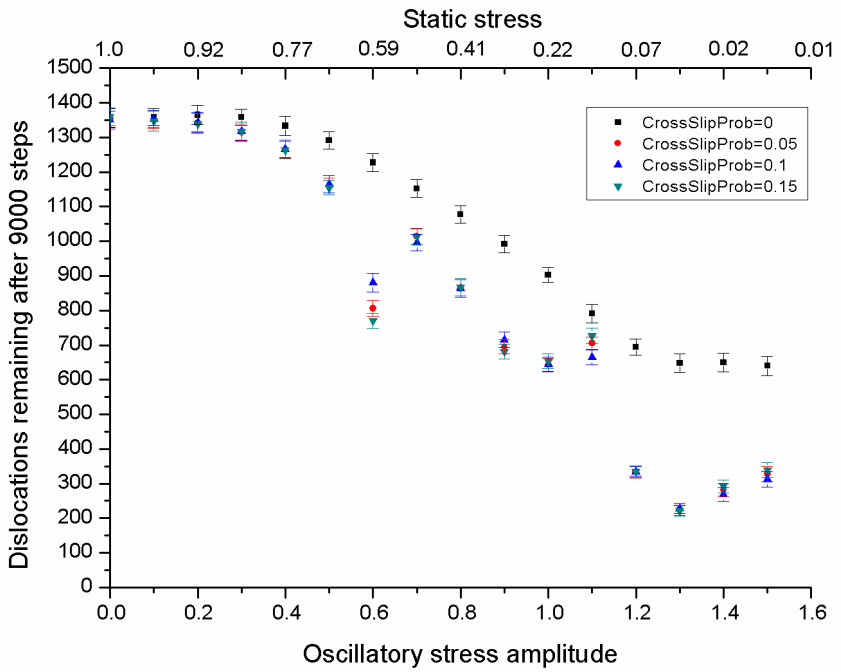
Static stress
1.0
0.92
0.77
0.59
0.41
0.22
0.07
0.02
0.01
Dislocations remaining after 9000 steps
Oscillatory stress amplitude
CrossSlipProb=0
CrossSlipProb=0.05
CrossSlipProb=0.1
CrossSlipProb=0.15

Fig. 5(b)

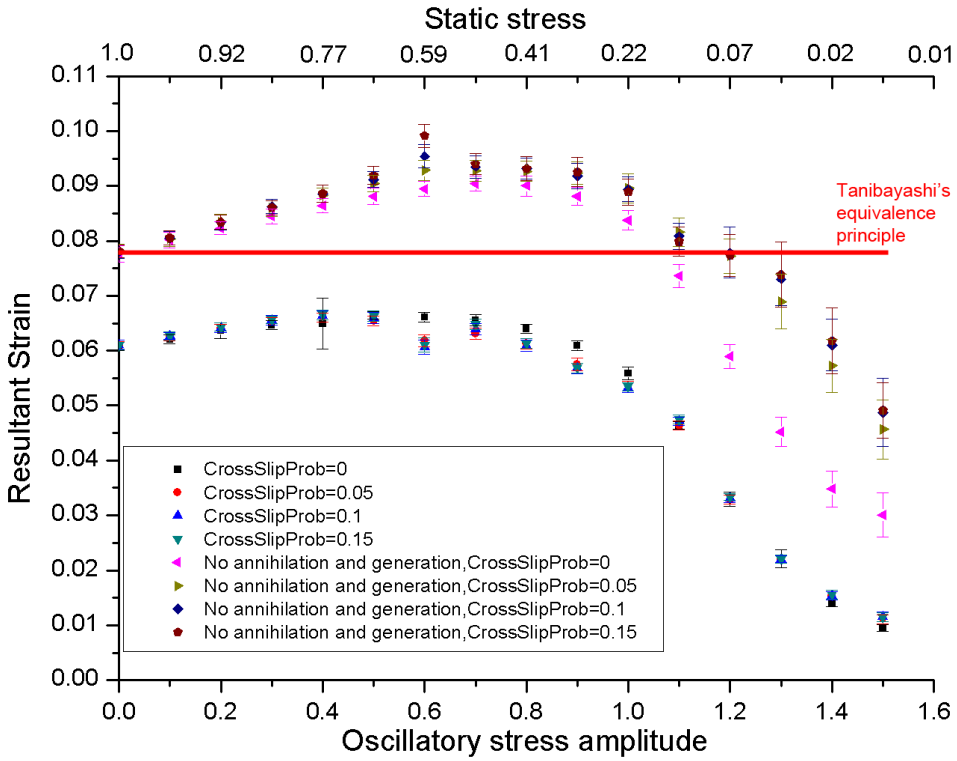
Static stress
Resultant Strain
Oscillatory stress amplitude
Tanibayashi's equivalence principle
CrossSlipProb=0
CrossSlipProb=0.05
CrossSlipProb=0.1
CrossSlipProb=0.15
No annihilation and generation,CrossSlipProb=0
No annihilation and generation,CrossSlipProb=0.05
No annihilation and generation,CrossSlipProb=0.1
No annihilation and generation,CrossSlipProb=0.15

Fig. 5(c)

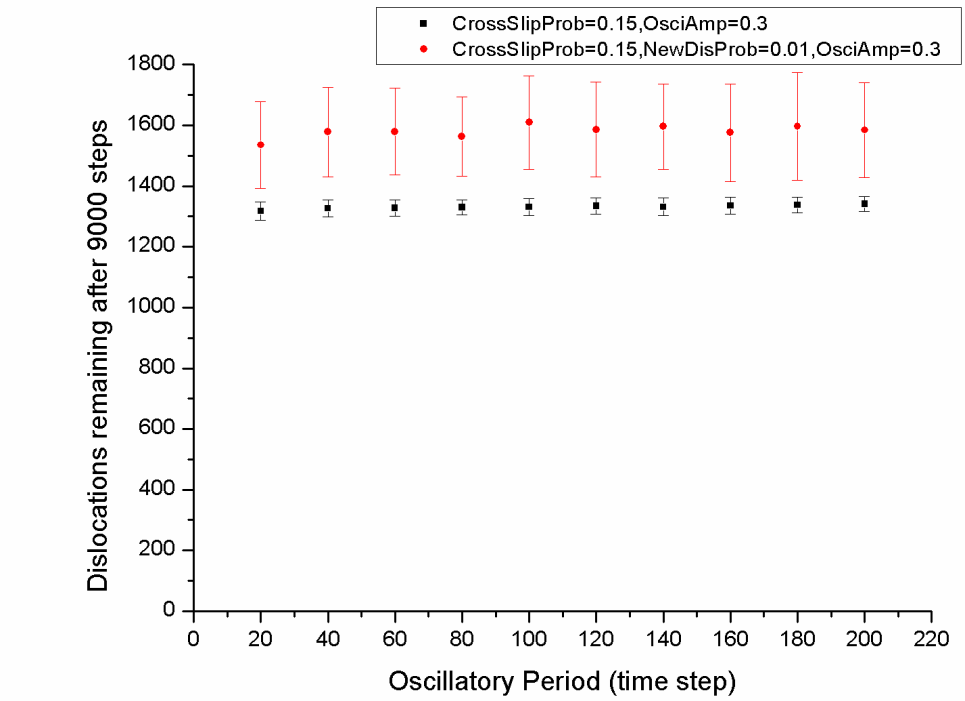
CrossSlipProb=0.15,OsciAmp=0.3
CrossSlipProb=0.15,NewDisProb=0.01,OsciAmp=0.3
Dislocations remaining after 9000 steps
Oscillatory Period (time step)
0
200
400
600
800
1000
1200
1400
1600
1800
0
20
40
60
80
100
120
140
160
180
200
220

Fig. 6

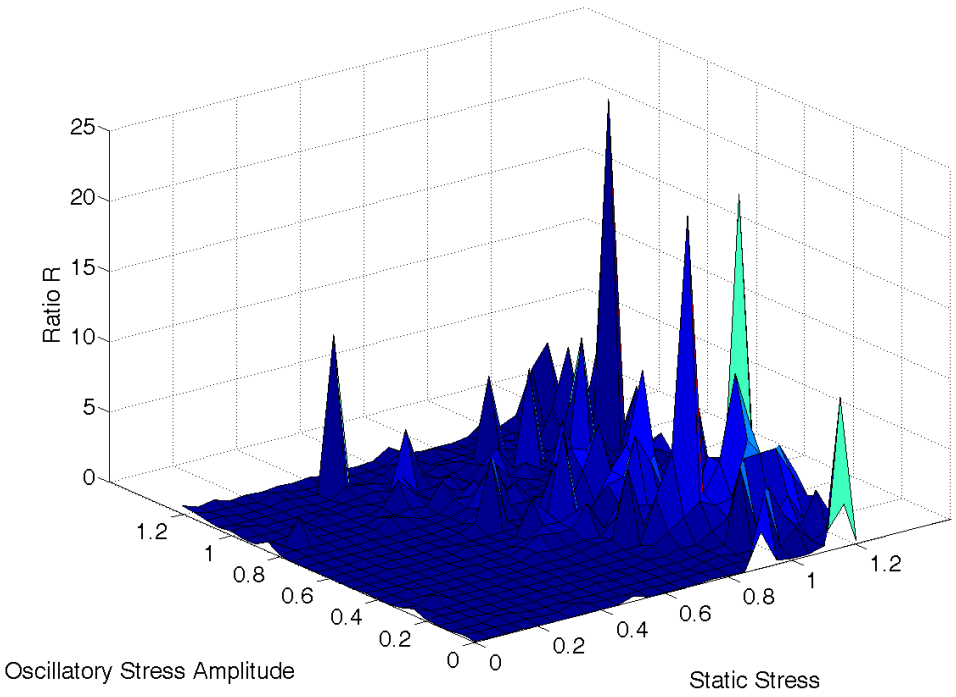
Ratio R
0
5
10
15
20
25
Oscillatory Stress Amplitude
0
0.2
0.4
0.6
0.8
1
1.2
Static Stress
0
0.2
0.4
0.6
0.8
1
1.2

Fig. 7